Evidence of Magnetostrictive Effects on STT-MRAM Performance by Atomistic and Spin Modeling

K. Sankaran[1], J. Swerts[1], R. Carpenter[1], S. Couet[1], K. Garello[1], R. F. L. Evans[2], S. Rao[1], W. Kim[1], S. Kundu[1], D. Crotti[1], G. S. Kar[1], and G. Pourtois[1, 3]
[1]imec, Leuven, Belgium, email: sankaran@imec.be,
[2]University of York, York, UK, [3]University of Antwerp, Antwerp, Belgium

***Abstract*—**For the first time, we demonstrate, using an atomistic description of a 30 nm diameter spin-transfer-torque magnetic random access memories (STT-MRAM), that the difference in mechanical properties of its sub-nanometer layers induces a high compressive strain in the magnetic tunnel junction (MTJ) and leads to a detrimental magnetostrictive effect. Our model explains the issues met in engineering the electrical and magnetic performance in scaled STT-MRAM devices. The resulting high compressive strain built in the stack, particularly in the MgO tunnel barrier (t-MgO), and in its associated non-uniform atomic displacements, impact on the quality of the MTJ interface and lead to strain relieve mechanisms such as surface roughness and adhesion issues. We illustrate that the strain gradient induced by the different materials and their thicknesses in the stacks has a negative impact on the tunnel magneto-resistance (TMR), on the magnetic nucleation process and on the STT-MRAM performance.

I. Introduction

In the new generation of stand-alone and embedded memories, the STT-MRAM, based on an out-of-plane magnetized MTJ (pMTJ), is a strong contender to conventional non-volatile memories [1]. The performance of a pMTJ is evaluated based on its magnetic and electric coupling that occurs through the CoFe|MgO|CoFe interface and its associated TMR and coercivity of the magnetic CoFe layer (Fig. 1a). Unfortunately, in the typical bottom-pinned TaN|Ru|CoPt |CoFeTa|CoFe|t-MgO|CoFe|CoFeTa|CoFe|c-MgO|CoFe|Ta|Ru |TiN stack (Fig. 1b), there is a strong discrepancy between the performance obtained on thin-film blankets and patterned devices (Fig. 1c). Indeed, the annealing process required to crystallize amorphous MgO (400°C during 90min) before the pattering step leads to a strong reduction of the device TMR and coercivity. Maintaining the structural integrity of this multi-material/layer device at the sub-nanometer scale is challenging due the differences in intrinsic mechanical properties and thermal expansion coefficients of the layers (see Fig. 2). Assuming a linear expansion for the materials, the expected mechanical strains induced by the thermal treatment in the different layers can be qualitatively assessed (Fig. 3 and inset). Among the different layers used in pMTJ devices, Ru undergoes the largest expansion with temperature, followed by MgO and CoFe (Fig. 3 inset), which leads to a highly non-uniform strain gradient. The system hence releases the strain through interfacial processes such as surface roughening, delamination, material lift off and diffusion [2]. These phenomena are enhanced during the patterning process after annealing.

This study aims i) understanding the consequences of a non-uniform strain gradient on the pMTJ performance, ii) drawing guidelines for material/device improvements and iii) establishing how the resulting perturbation of material interfaces impact on spin nucleation. For the first time, we report the presence of a non-uniform compressive strain profile in an etched STT-MRAM device of 30 nm diameter using atomistic simulations and show that that impacts on the CoFe|MgO interfaces and results in edge damage, as evidenced by TEM (Fig. 4). This leads to a significant lowering of the TMR with respect to the blanket case. We propose strategies to reduce this effect and use the atomistic structure of the pMTJ device as an input for spin modeling to quantify its consequences on the M-H hysteresis loop.

II. Methodology

First-principles simulations are performed by coupling density functional theory (DFT) with Non Equilibrium Green functions (NEGF) to compute the TMR in perfect epitaxial CoFe |MgO| CoFe stack [3]. The atomistic structures of the relaxed MTJ stack are obtained by minimizing the atomic forces with a conjugate gradient algorithm [4]. The interatomic potentials of each material and interfaces were described using the Buckingham-Coulomb and Lennard-Jones formalisms whose parametrizations were generated using a force-matching algorithm trained against DFT data [5] and carefully tested (Fig. 5). Atomistic spin simulations were performed using VAMPIRE [6], which combines a spin Hamiltonian to describe the energetics and the Landau-Lifshitz-Gilbert formalism for the spin dynamics.

III. Gate stack atomistic stucture

A. Atomistic model and experimental links

Starting from the film morphology built from an ideal epitaxial structure, the atomic structure of STT-MRAM devices has been built for a diameter of 30nm. The atomic forces of the stacks (Fig. 6a and b) have been relaxed with a conjugated gradient until the forces per atomic site reaches 10^{-4} eV/ Å (Fig. 6d). The relaxation process leads to significant changes in the atomic morphology (Fig. 6c) with respect to the ideal epitaxial case (Fig. 6a and b). These are consistent with cross-section TEM (Fig. 4a and b) profiles which report the occurrence of a strong roughness in the t-MgO [Fig. 4b I and Fig. 6c I] and the presence of edge damages (Fig. 4b II and Fig. 6c II). We also observe a strong diffusion of the Ru layer in contact with the

bottom TaN electrode (Fig. 4d III and Fig. 6c III) as evidenced by [7]. These deviations from the ideal structure are expected to impact significantly on device performance.

B. Atomic volume deformation and relation with the TMR

Those morphological changes induced by the relaxation of the epitaxial strain is captured by the atomic volume deformation (AVD) in the CoFe|MgO|CoFe layers which reflects the difference in atomic volume per site (computed using a Voronoi tessellation algorithm) between the relaxed and the epitaxial cases, see Fig. 7a. The latter clearly suggests that a strong compressive strain occurs in the pMTJ, particularly in the core part of the t-MgO. Although the TMR is a macroscopic effect of the pMTJ, a qualitative link can be established with the evolution of the TMR in epitaxial stacks under different hydrostatic deformations (Fig. 8) and the AVD of t-MgO. Using the AVD, we establish a qualitative mapping of the top surface of t-MgO and its intensity for different components of the TMR. Fig. 9 (middle) reveals that the parallel (Rp) and anti-parallel (Rap) resistances are increasing and the resulting TMR is significantly reduced with respect to the unstrained t-MgO (Fig. 9 top).

C. Impact of the top and bottom electrodes.

A similar exercise was repeated by removing the top TiN and bottom TaN electrodes. The AVD map suggests that the strain in the t-MgO layer (Fig. 10) comes with an important i) MgO edge lift-off (~5nm), ii) surface roughness and iii) an increase of Rp and Rap resulting in a low TMR (Fig. 9 bottom) compared the case where electrodes are present (Fig. 9 middle). This suggests that the mechanical compression from the electrodes prevents the t-MgO lift-off and that edge effects observed experimentally are not only related to etch issues.

IV. Stack Engineering

A. Single MgO vs. dual MgO vs. tripple MgO stack

The deposition of a top thin MgO capping (c-MgO) (<1.0nm) on top of the free-layer has been proposed to improve the thermal robustness and to increase of the free-layer coercivity [7]. Our simulations suggest that it also acts as a mechanical buffer which accommodates the compressive strain issued from the Ru layer and the top electrodes, where the expansion of the t-MgO stack with an additional c-MgO is hereafter referenced as being our process of reference (POR), Fig. 4c, 7 and 11. The utility of a thin c-MgO is further demonstrated by adding a third c-MgO cap on top of the POR. The resulting averaged compression in the t-MgO tunnel barrier is reduced from about -9.1 (t-MgO) to -8.1(t-MgO+1×c-MgO) and -5.3% (t-MgO+2×c-MgO) for the 30nm diameter device stack (Fig. 7b, c and 11). In the POR, the core of the MgO tunnel barrier is the object of a high compressive strain with respect to the edges, which is reduced by the introduction of a third c-MgO layer.

B. Impact of the top Ru thickness

It is also possible to reduce the compressive strain by optimizing the top Ru thickness (Fig. 12). As a proof of concept, we varied the Ru thickness from 5 (POR), to 2.5 and 10 nm. The resulting averaged strain sampled over the t-MgO tunnel barrier shows that a 2.5 nm thick Ru leads to similar profile as the (t-MgO+2×c-MgO) model (Fig. 12). Without any surprise, a thick Ru layer leads to a strong compressive strain (higher than in a single t-MgO). In that respect, reducing the thickness of the Ru layer is an excellent alternative to minimize the compression (Fig. 12) and to enhance the quality of the interface (Fig. 13).

C. Impact on the pMTJ interface

Figures 11, 12 and 13 summarize the overall interface quality of the pMTJ, which is assessed by quantifying the alignment of the CoFe|MgO interface by combining the Fe from CoFe and O from the MgO bond distortion and the amount of strain. Globally, changing the number of MgO layers in the stack has a limited impact on the interface quality, while it does strongly modulate the strain in the layer. On the other hand, the reduction of the thickness of Ru improves the interface quality by ~10% and reduces the strain (see Fig. 13).

V. Magnetic Responses of the strained pMTJ

The magnetic response of the atomic structure of the CoFe free-layer (Fig. 15 and 17 insets) and its M-H hysteresis loops were computed using atomistic spin dynamics simulations, which constitutes the ultimate limits of the discretization (Fig. 14). At low T (1K), both unstrained and strained free-layers show a perpendicular magnetization, while the coercivity of the strained one is reduced due to an easy magnetic reversal (Fig. 15). This is confirmed by the weak torque for the strained free-layer (Fig. 16). At room T, the strained free-layer adopts an in-plane magnetization due to the high disorder of the atomic sites (Fig. 17 and 18) and by the change in magnetic reversal mechanism induced by the strong thermal fluctuations and its associated spin modulations (Fig. 17 inset). This suggests that the magnetic response of the free-layer is considerably altered due to the non-uniform strain gradient in the stack.

VI. Conclusions

Our atomistic model suggests that a strong non-uniform strain gradient is present in STT-MRAM devices. This leads to detrimental magnetostrictive effects and a degradation in device performance. The minimization of the strain gradient built in the blanket layer upon patterning leads to edge effects such as a partial delamination of the tunneling barrier and a reduction of their active area. The introduction of additional thin MgO layers partially compensates for the strain gradient by reducing edge effects and minimizing the compressive strain accumulated in the MgO tunnel barrier. Reducing the thickness of the Ru layer has a similar effect. Our atomistic spin simulations suggest that the high disorder of the atomic sites in the CoFe free-layer leads to a strong perturbation of its magnetic response.

Acknowledgment

This work was carried out in the framework of the imec Core CMOS – MRAM Memory Program.

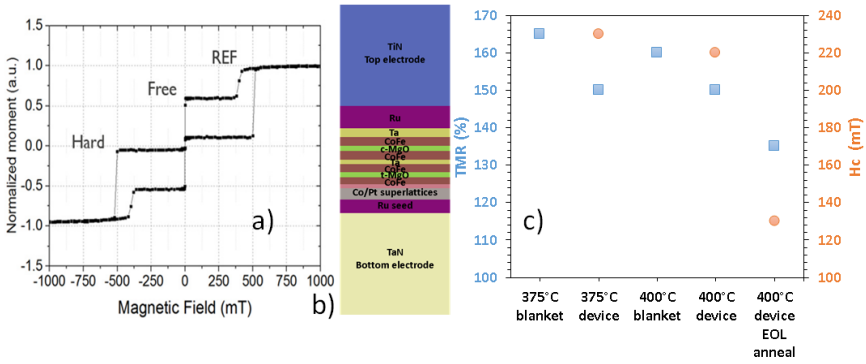

Fig. 1. a) Typical M-H loops of a STT-MRAM device. b) Schematic of the POR dual MgO with cap MgO (c-MgO) and tunnel MgO (t-MgO) device stacks. c) Experimental TMR (right) and free-layer coercivity (left) of blanket thin-film anneal and 45 nm electrical CD bottom-pinned devices anneal at 375 and 400°C.

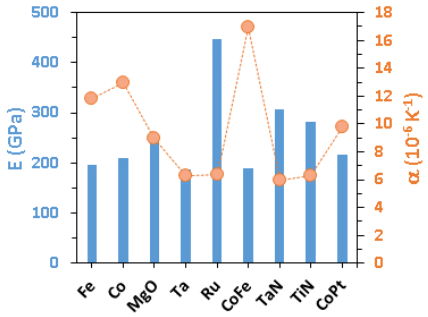

Fig. 2. Young modulus (histogram) and thermal expansion coefficient of the STT-MRAM constituting bulk materials.

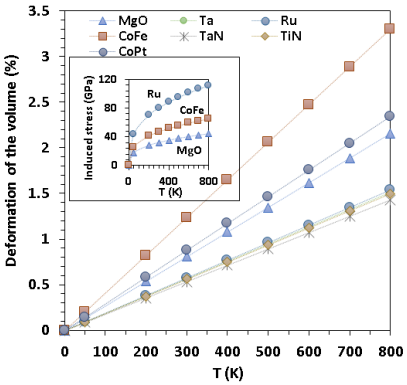

Fig. 3. Volume deformation expected upon thermal treatment based on bulk thermal expansion coefficients and Young modulus together with its induced stress for Ru, CoFe and MgO (inset).

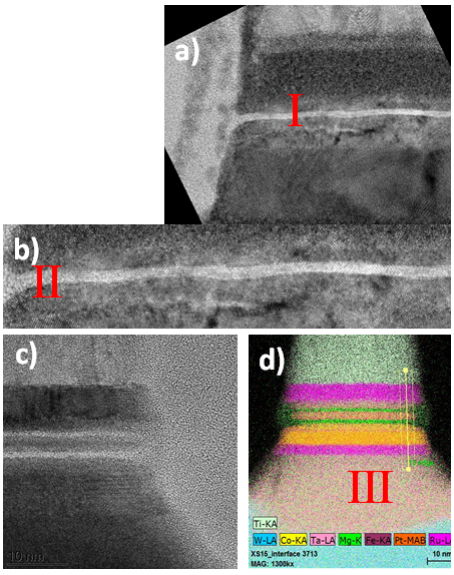

Fig. 4. a) TEM of a single MgO STT-MRAM device stack (a) and its zoomed in pMTJ image (b). (c) TEM of a dual MgO STT-MRAM stack after etch (without BEOL thermal treatment) and its EDX profile (d). I corresponds to interface roughness, II to the MgO lift-off, and III to Ru-TaN in-diffusion.

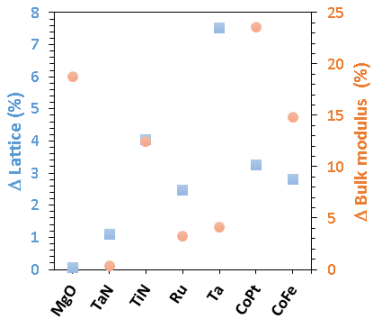

Fig. 5 Deviation of the computed lattice parameters and bulk Young modulus using the parametrized interatomic potentials with respect to DFT.

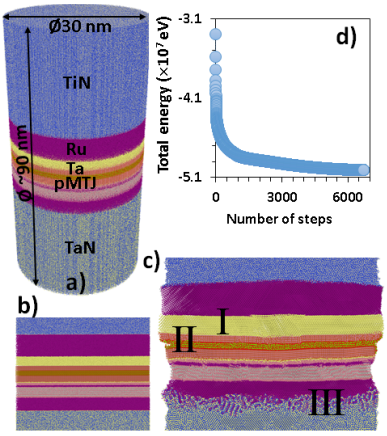

Fig. 6 Unrelaxed structure of the full STT-MRAM 30 nm diameter device (a). Transversal slice and zoomed view of stack before (b) and after (c) an atomic relaxation and the corresponding total energy minimization as a function of number numerical steps (d). I corresponds to the interface roughness, II to the MgO lift-off and III to Ru-TaN in-diffusion.

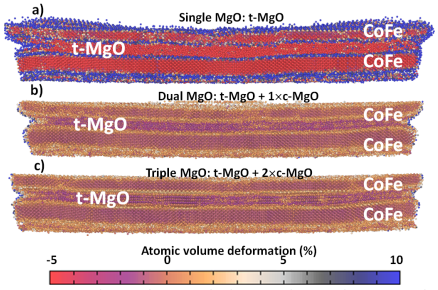

Fig. 7 Atomic volume deformation of pMTJ for a single MgO (a) [t-MgO], for a dual MgO (b) [t-MgO + 1×c-MgO] and for a triple MgO (c) [t-MgO + 2×c-MgO].

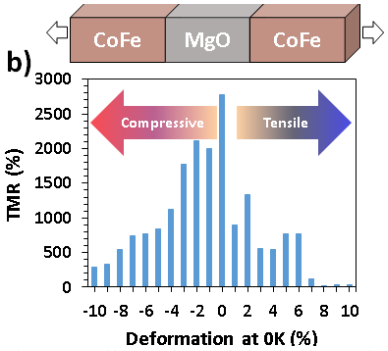

Fig. 8 a) Illustration of the hydrostatic deformations used to compute the TMR in epitaxial pMTJ stack. b) Resulting TMR obtained using DFT as a function of the strain applied in the pMTJ for an ideal CoFe|MgO|CoFe interface.

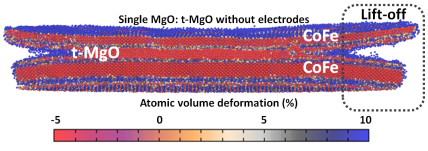

Fig. 10. Atomic volume deformation of the pMTJ of single MgO STT-MRAM of 30nm device without top and bottom electrodes.

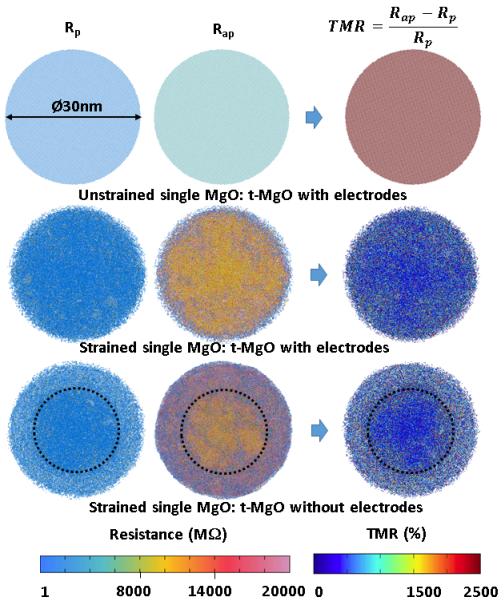

Fig. 9. Parallel (Rp), anti-parallel (Rap) resistance and TMR mapping (top view) of the pMTJ of single MgO device with and without electrodes.

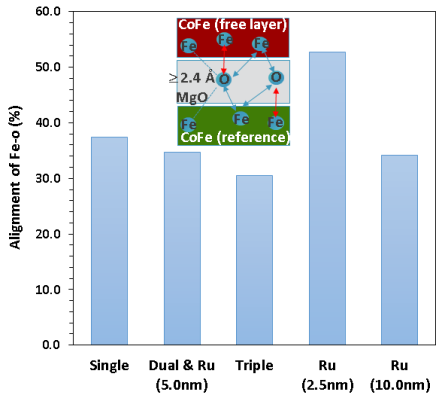

Fig. 13. Percentage of the available aligned Fe-O (see inset) at the interface of the pMTJ for different device stacks.

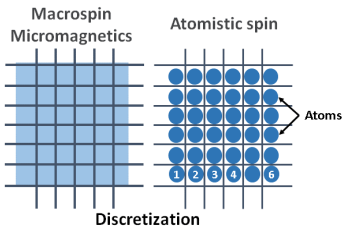

Fig. 14. Schematic description of the discretization for macrospin/ micromagetics and atomistic spin simulations.

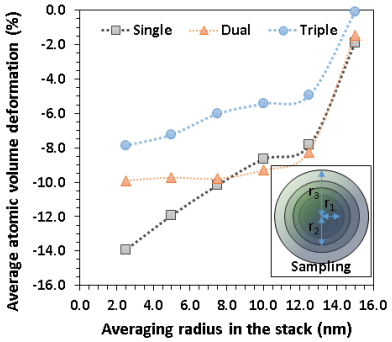

Fig. 11. Average atomic volume deformation of t-MgO in single, t-MgO+c-MgO and t-MgO+2 c-MgO) for 30nm diameter device as a function of the averaging radius r. The strain is sampled from the edge of the device to the center (inset).

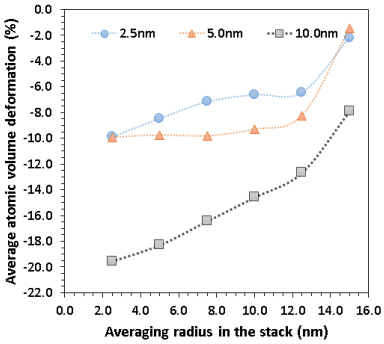

Fig. 12. Average atomic volume deformation of the MgO tunnel barrier in the dual MgO with Ru thickness of 2.5, 5.0 and 10nm STT-MRAM device of 30nm diameter as a function of the averaging radius in the stack (inset Fig. 11).

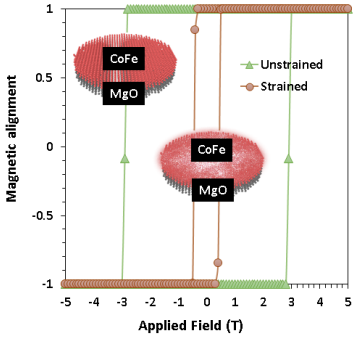

Fig. 15. M-H hysteresis loops at 1K of perfect epitaxial unstrained CoFe free-layer (top inset) compared with that of strained one (bottom inset).

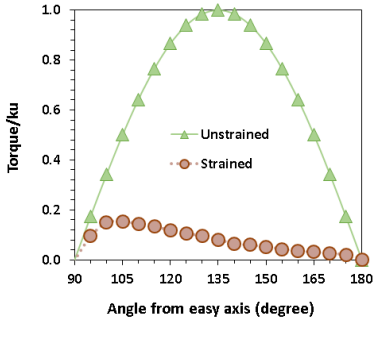

Fig. 16. Normalized torque at 1K of perfect epitaxial unstrained CoFe free-layer compared with that of the strained one.

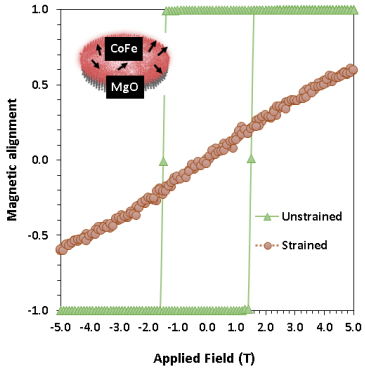

Fig. 17. M-H hysteresis loops at 300K of perfect epitaxial unstrained CoFe free-layer compared with that of strained one (inset schematics with random spin).

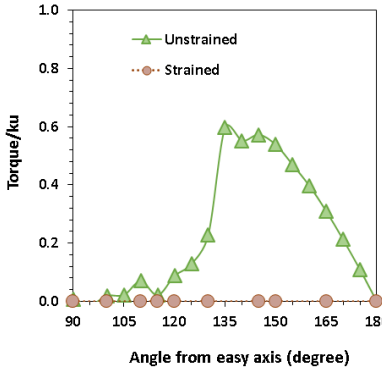

Fig. 18. Normalized torque at 300K of perfect epitaxial unstrained CoFe free-layer compared with that of the strained one.

REFERENCES

[1] S. Ikeda et al, "A perpendicular-anisotropy CoFeB-MgO magnetic tunnel junction" *Nat Mater.* 9, 721 (2010).
[2] J. Tersoff et al, "Competing relaxation mechanisms in strained layers" *Phys. Rev. Lett.*72, 3570 (1988).
[3] M. Brandbyge et al, "Density-functional method for nonequilibrium electron transport" *Phys. Rev. B* 65, 165401 (2002).
[4] S. Plimpton, "Fast Parallel Algorithms for Short-Range Molecular Dynamics" *J. Comp. Phys.* 117, 1 (1995).
[5] Brommer et al, "Classical interaction potentials for diverse materials from ab initio data: a review of potfit" *Modelling Simul. Mater. Sci. Eng.* 23, 074002 (2015).
[6] R. F. L. Evans et al, "Atomistic spin model simulations of magnetic nanomaterials" *J. Phys. Condens. Matter* 26, 103202 (2014).
[7] L. Wang et al, "Atomistic spin model simulations of magnetic nanomaterials" *Electrochem. Solid. S. Lett.* 15, H188 (2012).
[8] S.Couet etal, "Impact of Ta and W-based spacers in double MgO STT-MRAM free layers on perpendicular anisotropy and damping" *Appl. Phys. Lett.* 111, 152406 (2017).